Journal of Solid State Chemistry 196 (2012) 379–383

Contents lists available at SciVerse ScienceDirect

Journal of Solid State Chemistry

journal homepage: www.elsevier.com/locate/jssc

A high temperature neutron diffraction study of the double perovskite $Ba_2^{154}SmMoO_6$

Thomas K. Wallace [a], Clemens Ritter [b], Abbie C. Mclaughlin [a,*]

[a] Department of Chemistry, University of Aberdeen, Meston Walk, Aberdeen AB24 3UE, United Kingdom
[b] Institut Laue Langevin, 6 rue Jules Horowitz, BP 156, F-38042 Grenoble Cedex 9, France

ARTICLE INFO

Article history:
Received 2 April 2012
Received in revised form
19 June 2012
Accepted 20 June 2012
Available online 29 June 2012

Keywords:
Double perovskite
Phase transition
Neutron diffraction

ABSTRACT

Ba_2LnMoO_6 double perovskites have been recently shown to display a wide range of interesting magnetic and structural properties; $Ba_2^{154}SmMoO_6$ exhibits simultaneous antiferromagnetic order and a Jahn–Teller distortion. Here we report a high temperature neutron diffraction study of $Ba_2^{154}SmMoO_6$ from 353 to 877 K. The results evidence a tetragonal to cubic phase transition at 423 K. Above this temperature the thermal displacement parameters of the oxygen atoms are modelled anisotropically as a result of a transverse vibration of the bridging oxygen. A smooth increase in the cell parameter a is observed with temperature for $Ba_2^{154}SmMoO_6$.

1. Introduction

Perovskite related compounds are amongst the most widely studied because of their unique properties and versatile structure. With a general formula of ABX_3, the framework perovskite structure consists of a larger 12 coordinated A site cation and a smaller octahedrally coordinated B site cation, where X is usually oxygen. Cation ordering can occur on both A and B sites, however B site cation ordering is most commonly seen, leading to double perovskites of the form $A_2BB'X_6$ [1]. Ordering within the B site sub-lattice may adopt a layered or columnar pattern, however most commonly a rock salt configuration of B/B' cations is observed. Structural distortions can arise in perovskites in a number of ways; via ionic size effects leading to octahedral tilting [2,3] and through electronic phenomena such as the Jahn–Teller (JT) effect [4] and B site cation displacements [5]. As a consequence, perovskites commonly undergo distortions from the ideal cubic structure and are known to adopt tetragonal, orthorhombic, rhombohedral, monoclinic and triclinic structures [2,3].

Double perovskites of the form Ba_2REMoO_6 (where RE=rare earth) were originally synthesised by Brandle et al. [6]; however, without detailed analysis of their electronic or magnetic properties. Subsequent studies have highlighted a strong interplay between spin, lattice and orbital degrees of freedom in these compounds. In the perovskite manganites, such as $La_{1-\chi}Sr_\chi MnO_3$, a mixture of Mn^{4+} and Jahn–Teller active Mn^{3+} cations are present [7]. Strong JT distortions which are associated with unevenly filled e_g orbitals are thought to be key to the observation of colossal magnetoresistance in these materials. Conversely, Ba_2REMoO_6 compounds have singularly occupied Mo^{5+} t_{2g} orbitals which are susceptible to much weaker JT distortions [8,9]. Although this type of JT distortion is rare, it has been seen in a number of double perovskites such as the osmium double perovskite Ba_2NaOsO_6 [10], which shares the same $5d^1$ electron configuration seen in Ba_2REMoO_6. Such JT distortions may be static, where the lifting of orbital degeneracy is manifest in a structural distortion along a particular crystallographic direction; or they may be dynamic, whereby the orbital electron can occupy both high and low energy levels, resulting in an average of two distorted states.

Within the Ba_2REMoO_6 series all compounds are found to be electronic insulators with antiferromagnetic interactions between Mo^{5+} $s=1/2$ spins. In Ba_2REMoO_6 (RE=Gd–Yb, Y) [8,9,11] there is no evidence for magnetic order down to 2 K. Of these materials, Ba_2YMoO_6 has received particular attention as it is the first known instance of a valence bond glass (VBG) phase [12]. The VBG phase, which had been predicted theoretically [13], is characterised by a gradual freezing of spins into a disordered pattern of spin singlets. The ideal face centred cubic symmetry is maintained at all temperatures, resulting in Mo^{5+} orbital degeneracy down to 2 K. Within the structure, orbitally degenerate Mo^{5+} $s=1/2$ spins are geometrically frustrated as they are arranged on the corners of a lattice of edge sharing tetrahedra. This frustration drives the formation of spin singlet dimers; a fraction of the spins remain unpaired and are observed in magnetic susceptibility data and μSR measurements [12]. A subsequent study carried out on $Ba_{2-x}Sr_xYMoO_6$ found that

* Corresponding author. Fax: +44 122 427 2921.
E-mail address: a.c.mclaughlin@abdn.ac.uk (A.C. Mclaughlin).

0022-4596
http://dx.doi.org/10.1016/j.jssc.2012.06.030

the VBG phase persists despite a lowering of symmetry from cubic to monoclinic ($P2_1/n$) [14] which illustrates that the VBG phase is robust to structural distortions. Moreover, the coupling of the remnant fraction of $s=1/2$ spins at low temperature was found to change from paramagnetic for $x<2$ to ferromagnetic for $x=2$.

Magnetic studies of Ba_2NdMoO_6, Ba_2EuMoO_6 and $Ba_2^{154}SmMoO_6$ reported Néel ordering at $T_N=15$ K, $T_N=112$ K and $T_N=130$ K respectively [8,9,11]. Neutron diffraction studies of the Sm and Nd analogues evidence structural distortions from a higher temperature phase, described by the space group $I4/m$, to a lower temperature triclinic phase, described by I-1 symmetry. Whilst in $Ba_2^{154}SmMoO_6$ this structural distortion occurs at around 290 K, in Ba_2NdMoO_6 the same distortion occurs at the much lower temperature of 130 K [9]. Discrepancies were also observed in the nature of the JT distortion within these materials. In $Ba_2^{154}SmMoO_6$, simultaneous antiferrromagnetic and orbital ordering were seen at 130 K; whereas in Ba_2NdMoO_6, orbital ordering occurred over a 70 K temperature range from 130 to 60 K—well above T_N for this material so that there is a weaker correlation between orbital and magnetic ordering [9]. In both materials, below the Jahn–Teller transition, the single Mo^{5+} electron occupies both the d_{xz} and d_{yz} orbitals resulting in an elongation of the apical Mo–O bond length [8,9]. In order to further investigate the crystal structure into the high temperature regime, a variable temperature neutron diffraction experiment has been performed on the molybdenum double perovskite $Ba_2^{154}SmMoO_6$ between 353 and 877 K.

2. Experimental

Preparation of molybdenum double perovskites was carried out by solid state reaction of stoichometric amounts of MoO_3, $BaCO_3$ and $^{154}Sm_2O_3$ powder of 99% purity or higher. The $^{154}Sm_2O_3$ was supplied by Trace Sciences International and contained 98.9% ^{154}Sm, 0.6% ^{152}Sm, 0.1% ^{147}Sm, 0.1% ^{148}Sm, 0.2% ^{149}Sm and 0.1% ^{150}Sm. The use of the ^{154}Sm isotope was essential as ^{150}Sm has a high absorption cross section for neutrons. These oxides were ground and pelletised and then heated to 800 °C in an atmosphere of flowing 5% N_2/H_2 and held for 15 min, the temperature was then raised to 1000 °C and held for 15 min and then finally to 1200 °C and held for 4 h. Two further heat treatments were then carried out with intermediate grinding and pelleting to ensure sample homogeneity.

Phase purity was corroborated by laboratory X-ray diffraction, using a Bruker D8 Advance diffractometer with twin Goebel mirrors using Cu$K\alpha_1$ radiation. Variable temperature neutron diffraction patterns were recorded at a wavelength of 1.5943 Å on the superD2B diffractometer at the ILL, Grenoble, France. A 1 g sample was inserted into an 8 mm vanadium can and neutron diffraction patterns were recorded with an acquisition time of one hour over a range of temperatures between 353 and 877 K.

3. Results and discussion

Neutron diffraction data at all temperatures were fitted by the Rietveld method [15] using the software GSAS [16]. Modelling of the background was carried out with the linear interpolation function and peak shapes were modelled with a pseudo-Voigt function. Only the ^{154}Sm isotope was included in the refinement since the other isotopes were present in minor quantities. Refined atomic coordinates, isotropic/anisotropic thermal parameters, cell parameters, statistical measures of fit quality and selected bond lengths and angles are shown in Table 1. All of the metal and

Table 1
Refined atomic parameters for $Ba_2^{154}SmMoO_6$ (site occupancies, coordinates x, y, z and isotropic/anisotropic thermal parameters U) at selected temperatures. Atom positions at 353 K in the tetragonal $I4/m$ space group are Ba (0, 1/2, 1/4), Mo (0, 0, 1/2), ^{154}Sm (0, 0, 0), O(1) (0, 0, z), O(2) (x, y, 0). Atom positions in the cubic Fm-3m space group at temperatures above 353 K are Ba (1/4, 1/4, 1/4), Mo (1/2, 1/2, 1/2), ^{154}Sm (0, 0, 0), O(1) (x, 0, 0). Also tabulated are refined cell parameters, statistical measures of fit quality and selected bond lengths and angles.

Atom	Occupancy		Temperature (K)								
			353	423	493	563	633	703	777	837	877
Ba	1.00	U_{iso} (Å^2)	0.0128(3)	0.0149(3)	0.0167(3)	0.0183(3)	0.0273(3)	0.0231(3)	0.0241(3)	0.0259(4)	0.0273(4)
Mo	1.00	U_{iso} (Å^2)	0.0107 (8)	0.0015(4)	0.0082(5)	0.0081(6)	0.0090(6)	0.0103(6)	0.0110(6)	0.0118(7)	0.0118(7)
^{154}Sm	1.00	U_{iso} (Å^2)	−0.0001(5)	0.0066(5)	0.0021(4)	0.0033(4)	0.0042(5)	0.0051(5)	0.0061(5)	0.0063(5)	0.0074(5)
O(1)	1.00	x	–	0.23096(1)	0.23099(1)	0.23085(12)	0.23095(12)	0.23090(13)	0.23077(13)	0.23067(13)	0.23060(14)
		z	0.2690(6)	–	–	–	–	–	–	–	–
		U_{iso} (Å^2)	0.0291(1)	–	–	–	–	–	–	–	–
		U_{11} (Å^2)	–	0.0098(5)	0.0105(5)	0.0106(6)	0.0131(6)	0.0134(6)	0.0141(6)	0.0146(6)	0.0146(6)
		U_{22} (Å^2)	–	0.0309(4)	0.0337(4)	0.0359(4)	0.0383(4)	0.0411(5)	0.0436(5)	0.0460(5)	0.0475(5)
		U_{33} (Å^2)	–	0.0309(4)	0.0337(4)	0.0359(4)	0.0383(4)	0.0411(5)	0.0436(5)	0.0460(5)	0.0475(5)
O(2)	1.00	x	0.2503(5)								
		y	0.2847(7)	–	–	–	–	–	–	–	–
		U_{iso} (Å^2)	0.0091(12)								
		a (Å)	6.00616 (19)	8.50381(4)	8.50910(4)	8.51409(4)	8.51917(4)	8.52445(5)	8.52986(4)	8.53456(5)	8.53724(5)
		c (Å)	8.5052(5)	–	–	–	–	–	–	–	–
		χ^2	2.081	2.095	2.195	2.659	2.713	2.857	2.942	3.034	3.110
		R_{WP}	3.14	2.99	3.16	3.62	3.67	3.84	3.6	3.66	3.71
		R_P	2.42	2.3	2.42	2.74	2.73	2.89	2.63	2.66	2.69
		Mo–O(1) (Å)	1.964(5)	1.9644(13)	1.9672(14)	1.9671(14)	1.9669(15)	1.9682(15)	1.9686(15)	1.9708(15)	1.9699(16)
		Mo–O(2) (Å)	1.981(4)	–	–	–	–	–	–	–	–
		Sm–O(1) (Å)	2.288(5)	2.2865(13)	2.2862(14)	2.2890(14)	2.2916(15)	2.2925(15)	2.2951(15)	2.2953(15)	2.2975(16)
		Sm–O(2) (Å)	2.227(4)	–	–	–	–	–	–	–	–
		Mo–O(1)–Sm	180	180	180	180	180	180	180	180	180
		Mo–O(2)–Sm	172.1(2)	–	–	–	–	–	–	–	–
		Ba–O(1) (Å)	3.0074(3)	3.01091(5)	3.01276(5)	3.01460(5)	3.01635(6)	3.01825(6)	3.02022(6)	3.02193(6)	3.02291(6)
		Ba–O(2) (Å)	2.907(2)	–	–	–	–	–	–	–	–
		Ba–O(2) (Å)	3.114(2)	–	–	–	–	–	–	–	–

oxygen occupancies refined to within $\pm 1\%$ of full occupancy and were fixed to 1. There was no evidence for cation anti-site disorder or oxygen non-stoichiometry. Fig. 1 shows the Rietveld refinement fit to the neutron diffraction data of $Ba_2^{154}SmMoO_6$ recorded at 353 K, where a good fit was achieved with the tetragonal space group $I4/m$, [$a=6.00616(19)$ Å, $c=8.5052(5)$ Å, $\chi^2=2.081$, $R_{wp}=3.14\%$] in agreement with a previous neutron diffraction study on $Ba_2^{154}SmMoO_6$ at this temperature [8]. There is no evidence of peak splitting of the reflections intrinsic to the perovskite structure. Fig. 2 shows a portion of the 353, 423 and 493 K $Ba_2^{154}SmMoO_6$ neutron diffraction patterns, in the range 66°–78° 2θ. Above 353 K, the reduction in intensity of the (233) and (143) reflections is indicative of a structural phase transition to cubic symmetry. The intensities of the (233) and (143) reflections increase in the $I4/m$ space group as a result of the out of phase octahedral tilting described below. At the next temperature, 423 K, a good fit was achieved with the cubic Fm-3m space group [$a=8.50381(4)$ Å, $\chi^2=2.095$, $R_{wp}=2.99\%$]. Indeed, the Fm-3m cubic model resulted in an excellent fit at all temperatures above 353 K, up to the highest temperature of 877 K. The transition from high temperature cubic symmetry to lower temperature tetragonal symmetry is common in perovskites [17]. Structural distortions in perovskites can be driven by a number of phenomena from simple size effects to Jahn–Teller (JT) distortions and cation displacements. Application of the Goldschmidt tolerance factor, t, [18] to $Ba_2^{154}SmMoO_6$ results in a value of $t=0.98$, an indication that size effects drive the observed lowering of symmetry at 353 K. The ideal cubic perovskite structure occurs

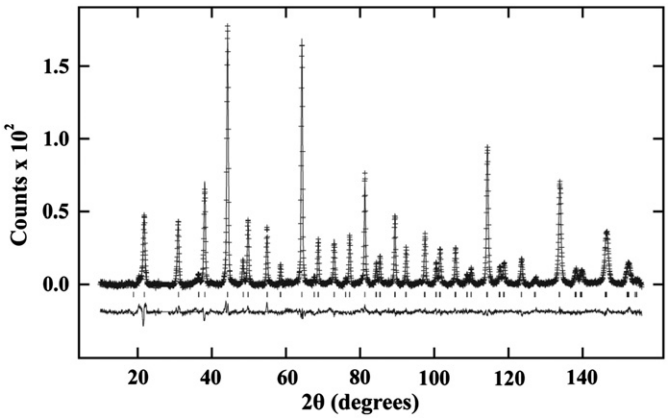

Fig. 1. Rietveld refinement fit to the 353 K neutron diffraction pattern of $Ba_2^{154}SmMoO_6$. Data is excluded in the 2θ range 26.5°–28.35° to account for a peak associated with the cryofurnace.

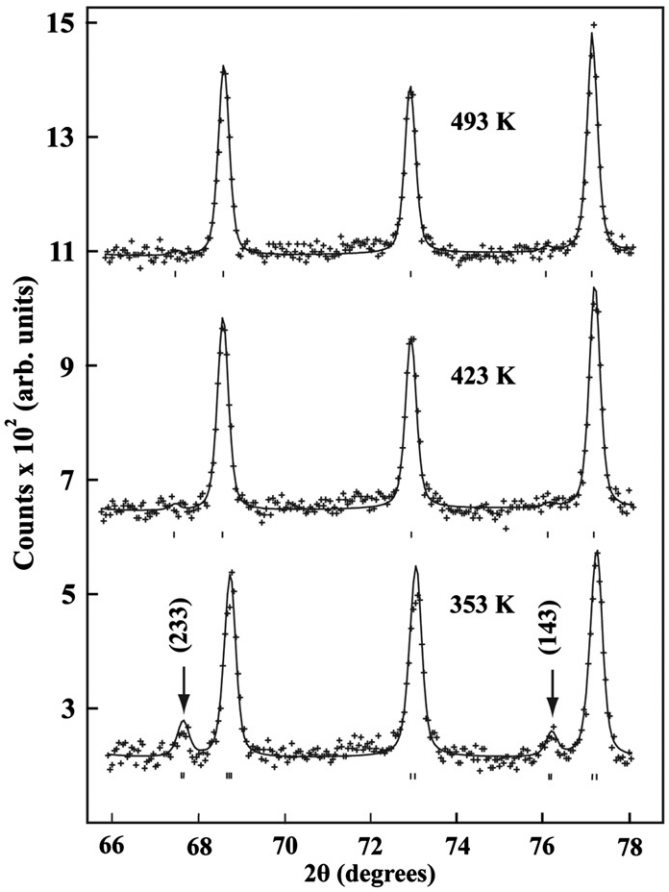

Fig. 2. A portion of the refined neutron diffraction pattern of $Ba_2^{154}SmMoO_6$ between 66° and 78° 2θ evidencing a cubic–tetragonal structural distortion between 423 and 353 K. Data is fit to the tetragonal $I4/m$ space group at 353 K and cubic Fm-3m above this temperature.

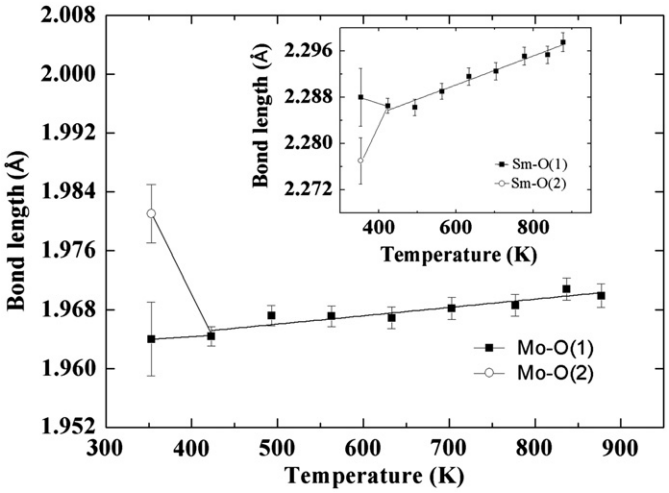

Fig. 3. Evolution of the Mo–O and Sm–O (inset) bond lengths with temperature in $Ba_2^{154}SmMoO_6$, showing a cubic–tetragonal structural transition at 353 K.

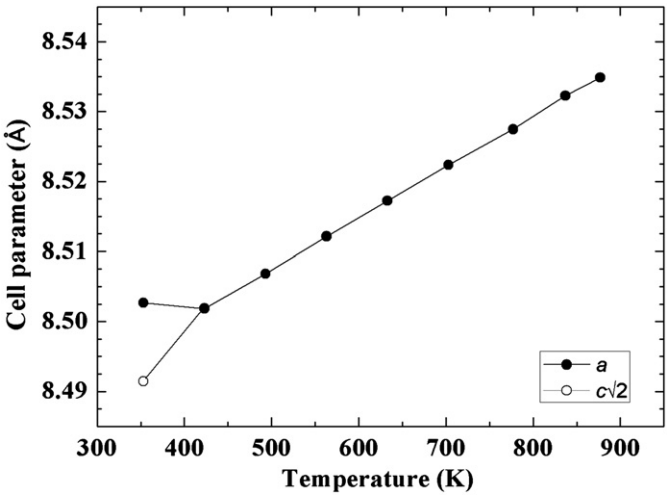

Fig. 4. Evolution of the cell parameters with temperature in $Ba_2^{154}SmMoO_6$ evidencing a structural distortion at 353 K, c is multiplied by $\sqrt{2}$ for comparison purposes.

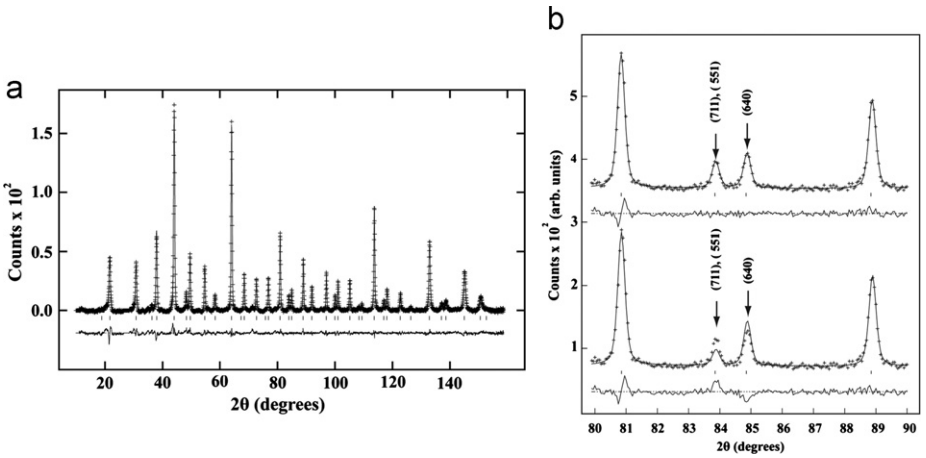

Fig. 5. (*a*) Rietveld refinement fit to the 777 K neutron diffraction pattern of $Ba_2^{154}SmMoO_6$. Data is excluded in the 2θ range 26.5°–28.35° to account for a peak associated with the cryofurnace; (*b*) A portion of the 777 K neutron diffraction pattern of $Ba_2^{154}SmMoO_6$ between 80° and 90° 2θ, (above) showing the fit with anisotropic oxygen thermal parameters, (below) the fit with isotropic oxygen thermal parameters.

in the circumstance $t=1$, and when $t\neq 1$, distortions from the ideal structure occur. It is known that when $t<1$, *B*–O and *B*′–O bonds within the structure are compressed, whilst *A*–O bonds are stretched [5] and octahedral rotations and tilts occur to alleviate stress. In $Ba_2^{154}SmMoO_6$, the observed cubic (*Fm*-3*m*) to tetragonal (*I*4/*m*) phase transition occurs due to rotations of octahedra about the cubic (001) axis and can be described by the Glazer tilt system ($a^0a^0c^-$) in corroboration with a recent group theoretical analysis of structural distortions of double perovskites [3].

The observed reduction in symmetry between 353 and 423 K is also reflected in the evolution of Mo–O and Sm–O bond lengths with temperature (Fig. 3). The structural phase transition occurring at 353 K is highlighted by the Mo–O bond lengths, where a shortening of the Mo–O(1) bond lengths and an elongation of the Mo–O(2) bond lengths occurs. This evolution of the bond lengths is consistent with the rotations of octahedra in the (001) plane. Above 353 K, in the cubic regime, there is an approximately linear expansion of the Mo–O bond lengths with increasing temperature as would be expected with increasing thermal energy. The evolution of the Sm–O bond lengths with temperature is displayed in the inset to Fig. 3; an expansion of the Sm–O bond lengths is evidenced with increasing temperature. At the cubic–tetragonal transition, an expansion of Sm–O(1) and a shortening of Sm–O(2) is observed, as a result of rotations of the SmO_6 octahedra. The evolution of cell parameters with temperature is shown in Fig. 4 and a smooth increase in *a* is observed as the temperature is increased from 423 to 877 K.

Above the tetragonal to cubic phase transition, considerably better agreement between the observed and calculated patterns was obtained when the oxygen atom's thermal parameters were refined anisotropically rather than isotropically. Fig. 5*a* shows the Rietveld refinement fit of data recorded at 777 K, where a good fit was achieved with the cubic (*Fm*-3*m*) model. Fig. 5*b* shows a portion of the 777 K refinement data between 80°–90° 2θ, and highlights the improvement to the fit by the introduction of anisotropic oxygen thermal parameters; an intensity mismatch is clearly seen at the (711), (511) and (640) reflections. This improvement to the fit is reflected in the statistical measures of fit quality: $\chi^2=3.849$ and $R_{wp}=4.12\%$ (modelling the oxygen thermal parameters isotropically) and $\chi^2=3.102$ and $R_{wp}=3.7\%$ (modelling the oxygen thermal parameters anisotropically). Fig. 6 shows the thermal ellipsoids of the oxygen atoms within the $Ba_2^{154}SmMoO_6$ cubic structure at 423 K. The oxygen atoms have their largest displacement amplitudes perpendicular to the linear Mo–O–Sm bonds and the displacement amplitudes increase as the temperature is raised. This corresponds to a transverse vibration which is commonly observed in tungstates such as ZrW_2O_8 and $Sc_2W_3O_{12}$ [19].

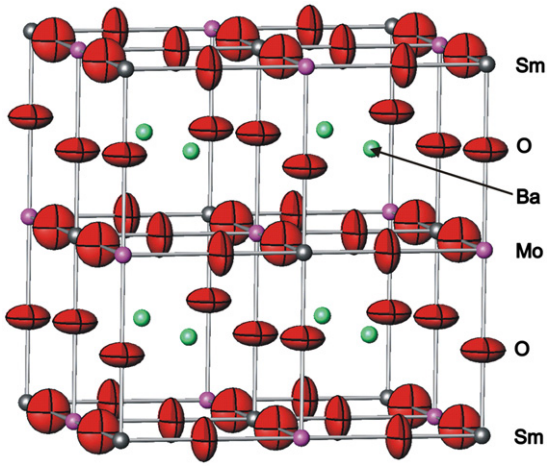

Fig. 6. The crystal structure of $Ba_2^{154}SmMoO_6$; Sm, Mo, Ba and O atoms are labelled. The ellipsoids on the oxygen sites evidence a transverse thermal motion.

4. Conclusions

In summary, we have investigated the high temperature crystal structure of $Ba_2^{154}SmMoO_6$. Results show that there is a phase change from tetragonal *I*4/*m* symmetry to cubic *Fm*-3*m* at 423 K. The best fit to the cubic model is obtained by modelling the thermal parameters of the oxygen atoms anisotropically which evidences a transverse thermal motion of the bridging oxygens throughout the structure. The amplitude of this thermal motion increases as the temperature rises from 423 to 877 K.

Acknowledgments

We acknowledge STFC for beam time provision and the University of Aberdeen for provision of a studentship (TKW).

References

[1] G. King, P.M. Woodward, J. Mater. Chem. 20 (2010) 5785–5796.

[2] P.M. Woodward, Acta Crystallogr. 53 (1997) 32–43.
[3] C.J. Howard, B.J. Kennedy, P.M. Woodward, Acta Crystallogr. B59 (2003) 463–471.
[4] A.J. Millis, B.I. Shraiman, R. Mueller, Phys. Rev. Lett. 77 (1996) 175.
[5] J.B. Goodenough, Rep. Prog. Phys. 67 (2004) 1915–1993.
[6] C.D. Brandle, H. Steinfink, Inorg. Chem. 10 (1971) 922.
[7] G.H. Jonker, J.H. Van Santen, Physica 16 (1950) 599–600.
[8] A.C. Mclaughlin, Phys. Rev. B 78 (2008) 132404.
[9] E.J. Cussen, D.R. Lynham, J. Rogers, Chem. Mater. (18, 2006) 2855–2866.
[10] A.S. Erickson, S. Misra, G.J. Miller, R.R. Gupta, Z. Schlesinger, W.A. Harrison, J.M. Kim, I.R. Fisher, Phys. Rev. Lett. 99 (2007) 016404.
[11] A.C. Mclaughlin, Solid State Commun. 137 (2006) 354–357.
[12] M.A. de Vries, A.C. Mclaughlin, J.-W.G. Bos, Phys. Rev. Lett. 104 (2010) 177202.
[13] M. Tarzia, G. Biroli, Europhys. Lett. 82 (2008) 67008.
[14] A.C. Mclaughlin, M.A. de Vries, J.-W.G. Bos, Phys. Rev. B 82 (2010) 094424.
[15] H. Rietveld, J. Appl. Cryst. 2 (1969) 65–71.
[16] A.C. Larson , R.B. Von Dreele, Los Alamos National Report Laboratory Report no. LA-UR-86-748, 1994.
[17] A.M. Glazer, Acta Crystallogr. 28 (1972) 3384–3392.
[18] V.M. Goldschmidt, Naturwissenschaften 14 (1926) 477–485.
[19] A.W. Sleight, Inorg. Chem. 37 (1998) 2854–2860.